MEASUREMENT OF LAMINAR VELOCITY PROFILES IN A PROTOTYPIC PWR FUEL ASSEMBLY

S. Durbin[a,*], E. Lindgren[a], and A. Zigh[b]

[a] *Sandia National Laboratories*
[b] *Nuclear Regulatory Commission*

Abstract

Laminar gas flow in a nuclear fuel assembly is of interest for complete loss-of-coolant accident scenarios in spent fuel pools and for performance analyses of dry storage casks. For this study, velocity profiles were measured across the bundle of a prototypic pressurized water reactor (PWR) fuel assembly using a laser Doppler velocimeter (LDV). The results for two containment cells representative of values spanning pool and cask cells available in industry are reported here. The apparatus was tested in what is traditionally considered the laminar regime for Reynolds numbers equal to 100 and 900, based on the average assembly velocity and hydraulic diameter.

Mixing vanes present in the spacers and intermediate fluid mixers were observed to impart long-lived wake disturbances into the flow as evidenced by non-zero root-mean-square fluctuations in the flow. These fluctuations do not appear to influence the mean velocity profiles as compared to the fully-developed laminar solution at *Re* = 100. However, the mean velocity profiles at *Re* = 900 show significant deviation from laminar simulations. These results suggest that flows inside PWR fuel assemblies of *Re* = 100 to 900 may be more aptly described by transitional or turbulent computational fluid dynamics (CFD) modelling.

1. INTRODUCTION

Low Reynolds number flows in spent nuclear fuel are found in dry cask storage canisters and are expected in postulated, complete loss-of-coolant accidents. These assemblies have been designed for operation in the turbulent flow regime. As such, most of the available literature focuses on the performance and analysis of fuel assemblies and components in turbulent flow.

Several investigators have examined the effects of spacers on the flow inside of a fuel bundle. Rehme and Trippe (1980) examined the velocity distribution in triangular arrayed rod bundles with various rod pitches and spacer blockage ratios using Pitot tubes for *Re* = 15,000 to 90,000. More recently, Dominguez-Ontiveros and Hassan (2009) have conducted studies using particle image velocimetry to measure the two-dimensional flow field in a square array bundle with swirl type spacers at *Re* = 6,400. They concluded that the spacers acted to attenuate the vorticity present in the flow.

Similar to this study, Caraghiaur et al. (2009) used LDV to explore the velocity within a square rod bundle with spacer grids at Re = 25,000 to 42,000. Caraghiaur determined that the turbulence intensity initially decreases downstream of the spacer grid for subchannels within the bundle and reaches a peak value at approximately two spacer lengths before decaying. The wall subchannel did not display the initial depression in turbulence intensity, instead peaking just downstream of the spacer followed by monotonic decay. Furthermore, Caraghiaur concluded that turbulence enhancements from spacer effects are not exclusively dependent upon the local geometric details of the spacer in the subchannel. Chang et al. (2008) also used LDV to investigate the flow within a square array rod bundle with spacers of different mixing vanes for *Re* = 48,000. For the split type mixing vanes like the ones in this study, Chang found that strong vorticity was introduced into the flow immediately downstream of the spacer. This vorticity was short lived, being greatly reduced within four hydraulic diameters downstream of the spacer.

[*] Corresponding author
Email address: sdurbin@sandia.gov

CFD simulations have had moderate success in modelling the flow within PWR bundles with spacers. Among others, Lee and Choi (2007) were able to successfully model a 17×17 PWR assembly complete with various types of mixing vanes at *Re* = 542,000. This modelling effort used the Reynolds stress model for closure.

2. EXPERIMENTAL SETUP

The apparatus was constructed from a commercial PWR fuel "skeleton" and stainless steel tubing with the assembly in a vertical orientation. The stainless steel tubing functioned as surrogate fuel pins and had prototypic top and bottom fuel plugs. The skeleton included the top and bottom nozzles, debris catcher, guide tubes, fuel spacers, and intermediate flow mixers. Each containment cell was constructed from stainless steel on three sides and an acrylic window along the length of the remaining side. Metered, dry air at ambient conditions was forced into the bottom of the assembly through a flow conditioner. The LDV was arranged perpendicular to the optical window, and velocity traverses were taken in between the rows of simulated fuel rods. Different axial positions of interest were investigated including pre-spacer, post-spacer, and mid-bundle locations.

All experiments were conducted at isothermal conditions. The assembly was oriented vertically with respect to gravity, as in spent fuel pools and vertical spent fuel casks. Details of the air flow system are available in Lindgren and Durbin (2010). The original experimental setup and details are documented in Durbin and Lindgren (2008).

2.1 Fuel Assembly

The highly prototypic fuel was modelled after a commercially available 17×17 PWR assembly. Commercial components were purchased to create the assembly including the top and bottom nozzles, spacers, intermediate fluid mixers (IFM), 24 guide tubes, one central instrumentation tube, and all related assembly hardware. The mixing vanes of the spacers and IFMs were of the small scale vortex flow, or split type. Many of these components are pictured in Fig. 1. The central instrumentation tube and guide tubes are permanently attached to the spacers to form the structural skeleton of the assembly.

Stainless steel tubing was substituted for the fuel rod pins for hydraulic testing. The diameter of the stainless steel rods was slightly larger than prototypic pins, 9.525 mm versus 9.500 mm. Prototypic fuel rod end plugs supplied by the fuel vendor were press fit into the ends of the stainless tubing. The guide tube diameter was 12.2 mm, and the pin pitch was 12.6 mm.

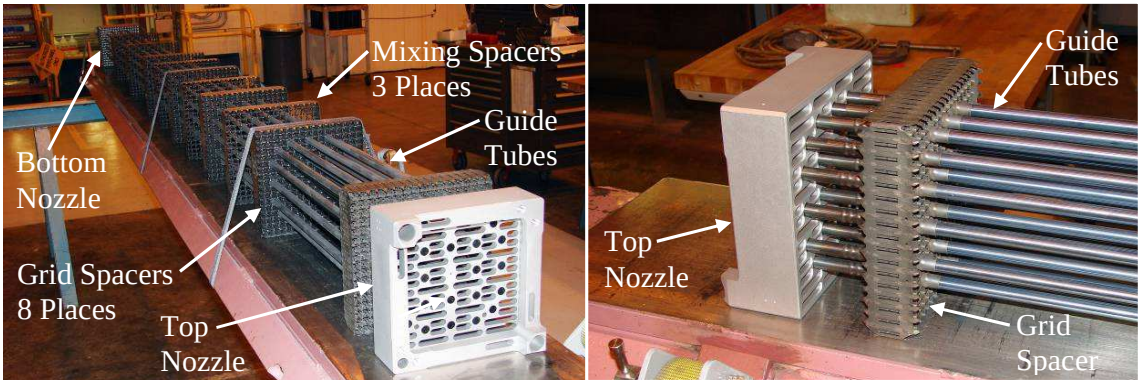

Fig. 1: Prototypic 17×17 PWR components.

2.2 Storage Cells

The extent of the gap between the outer row of rods and the inside cell wall influences the nature of flow inside the bundle. In order to study this effect, two different sized storage cells were examined for this effort. These two sizes were chosen to represent one of the larger, common commercial sizes and one tight-fitting cell size that minimized the annular flow. Table 1 lists the dimensions of cells

used in these studies as well as two Holtec dry casks and a typical Holtec pool rack for reference. The outer dimension of the 17×17 spacer is 214.0 mm, which is the smallest possible storage cell that would fit on the assembly. The internal dimensions of the listed commercial cells range considerably from a low of 222.2 mm to a high of 226.6 mm.

Since there is variation in the size of the cells used commercially, two different sized pool cells were tested as indicated in gray in Table 1. Although the 217.5 mm size is not found commercially, it is an important case for comparison purposes as it minimizes the complexity of the annular gap flow. The other experimental storage cell size of 226.6 mm is that like found in the Holtec MPC-24 cask. This span of sizes includes the size used in a typical Holtec spent fuel pool rack.

Table 1: Summary of the reference flow areas and hydraulic diameters of commercial cask, pool cells, and areas of as-built experimental cells.

Type	Storage Cell Dimension (mm)	Flow Area (m^2)	Hydraulic Diam., D_H (m)
Exp. Storage Cell 1	217.5	0.0256	0.0105
Exp. Storage Cell 2	226.6	0.0296	0.0121
Holtec MPC-24E/EF	222.2	0.0276	0.0113
Holtec MPC-24	226.6	0.0296	0.0121
Holtec Pool	224.8	0.0288	0.0118

2.3 Laser Doppler Velocimetry Measurements

The average velocity and root-mean-square (RMS) velocity fluctuations were measured in these experiments by a single-component laser-Doppler anemometer (Dantec 1-D FlowExplorer). This LDA system is composed of the FlowExplorer probe head, a photomultiplier, a burst analyzer, a motorized stage and controller unit, a PC-based data acquisition (DAQ) system, and data processing software.

Fig. 2 shows the layout of the test components for LDA measurements. The LDA probe was mounted externally to the PWR assembly on two manual stages (*z*- and *y*-axis control) and a single motorized stage (*x*-axis control). The laser beams pass through the optical window into the assembly and measure the velocity at the intersection of the beams. In this manner the local velocity can be measured across the assembly in between rod banks. All measurements in this report were recorded at $y = 94.5$ mm, or in the middle of the first and second rod banks. This position was chosen to avoid the smaller clearances between guide tubes and fuel pins. Also, the influence of the cell wall, which is of interest in these studies, is greater at this location than between the seventh and eighth rod banks $y = 18.8$ mm. All profiles were taken from the cell wall to the mid-plane of the bundle, $x = 0$ mm. The three axial locations investigated are $z = 1.326$, 1.537, and 2.787 m corresponding to post-spacer, mid-bundle, and pre-spacer positions in the bundle, respectively. These locations are 3.7 and 3.2 hydraulic diameters (pre-spacer), 3.5 and 3 hydraulic diameters (post-spacer), and 23.6 and 20.5 hydraulic diameters from the spacer grids for the 217.5 and 226.6 mm cells, respectively. Fig. 3 gives two photographs of the LDA setup. These photographs depict a measurement just inside the optical window.

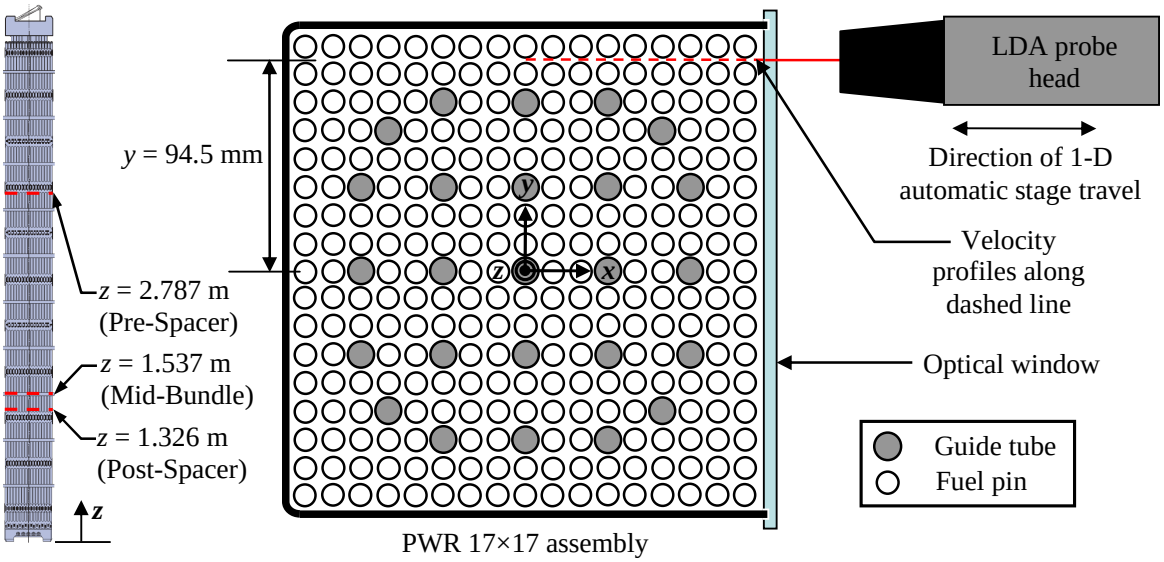

Fig. 2: Schematic of the LDA system for measuring velocity profiles in the PWR 17×17 assembly.

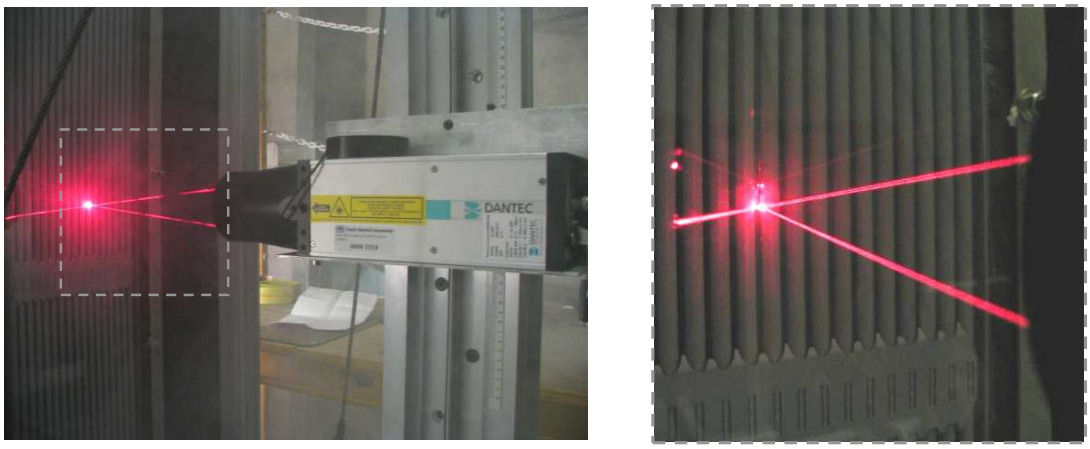

Fig. 3: Photographs showing the LDA probe system in relation to the fuel assembly.

3. RESULTS

3.1 Comparison with Laminar Simulations

The measured, time-averaged velocities (symbols) for the 217.5 mm cell are plotted against the corresponding fully-developed laminar solutions (lines) at *Re* = 100 (red) and 900 (blue) in Fig. 4. The measurements are from the mid-bundle location in the assembly (z = 1.537 m). A FLUENT model with the same bundle geometry was used to generate the fully-developed laminar solutions. A uniform velocity profile was introduced into the bottom of the laminar model with the same bulk average bundle velocity, W_o, as in the experiment. The laminar velocity profiles were checked for convergence to the fully-developed condition by examining profiles significantly downstream from the model inlet. The geometry of the spacer grids was not modelled. These FLUENT solutions are presented as a reference to demonstrate the deviation of the actual data from the ideal laminar flow profile. Uncertainty limits corresponding to a 95% confidence level are shown for each measurement. The uncertainty is primarily due to uncertainty in the mass flow controllers used to meter the air into the assembly. The uncertainties for *Re* = 900 are smaller than the symbols.

Measurements are not reported for positions between x of ~100 to 108.75 mm due to poor signal quality. The time-averaged velocities agree within experimental uncertainty at *Re* = 100. However,

the measured velocity profile at *Re* = 900 differs significantly from the laminar solution. The maxima and minima are reduced more than predicted from strictly laminar flow, indicating enhanced mixing from the spacers.

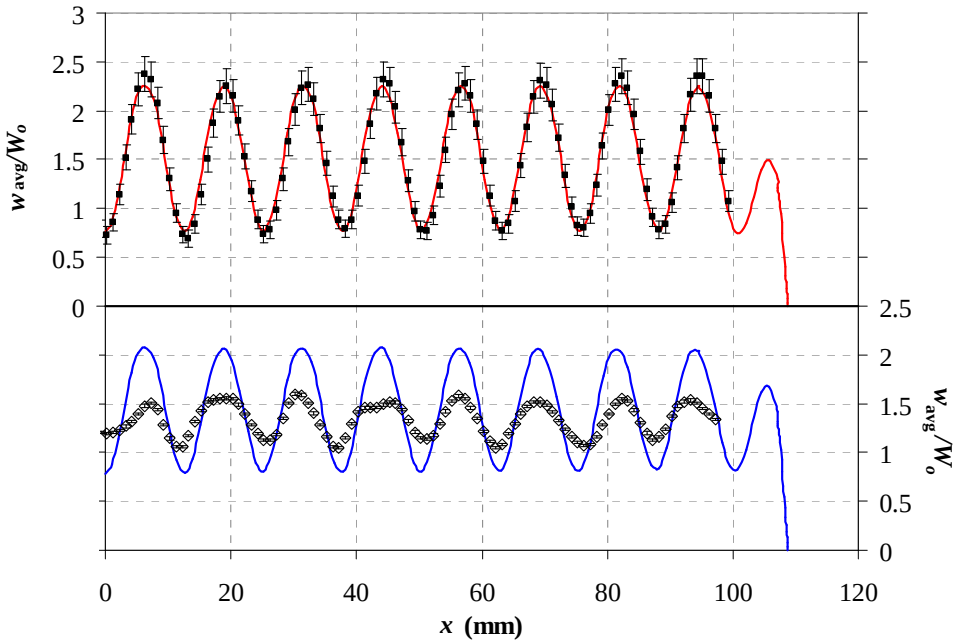

Fig. 4: Normalized mean velocity profiles for the 217.5 mm cell at *Re* = 100 (red) and 900 (blue) for fully-developed laminar (lines) and LDV measurements (symbols).

Fig. 5 shows the normalized mean velocity profiles for the 226.6 mm cell at *Re* = 100 (red) and 900 (blue) for fully-developed laminar (lines) and LDV measurements (symbols). The velocity profiles are again normalized by the bulk average bundle velocity, W_o. The velocity is underpredicted for both Reynolds numbers in the wall subchannel. The laminar velocities for *Re* = 100 in the interior subchannels are slightly higher than the measurements. Again, the velocity profile at the higher Reynolds number is distorted towards a more uniform distribution as compared to the laminar profile. These effects demonstrate the influence of the spacers on the distribution of flow away from the idealized laminar case.

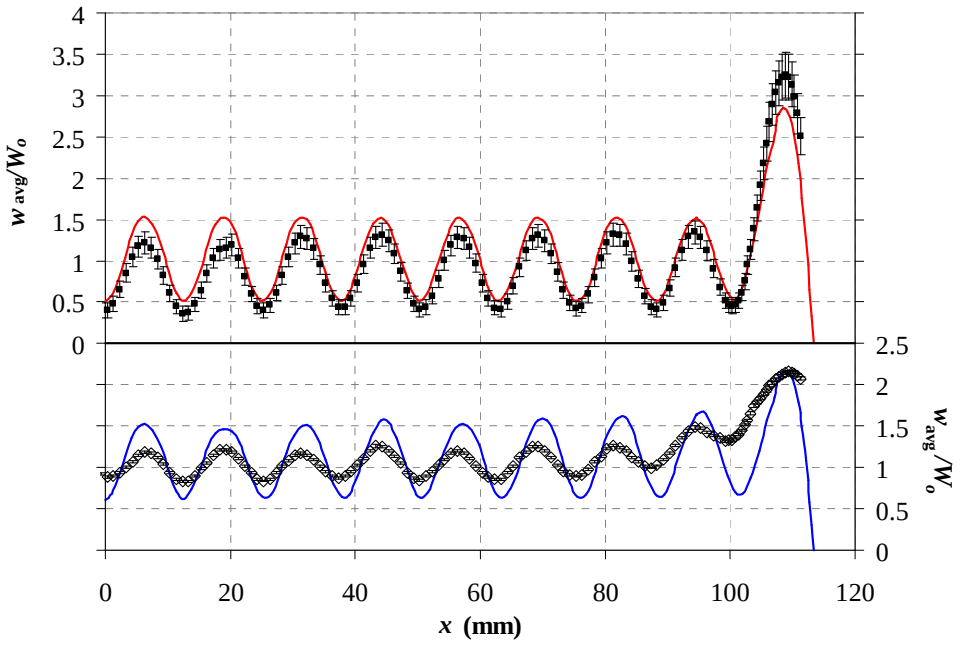

Fig. 5: Normalized mean velocity profiles for the 226.6 mm cell at *Re* = 100 (red) and 900 (blue) for fully-developed laminar (lines) and LDV measurements (symbols).

3.2 Laser Doppler Velocimetry Measurements

Normalized mean and root-mean-square (RMS) velocity fluctuation profiles of the 217.5 mm cell for *Re* = 100 are shown in Fig. 6. The local time-averaged velocity in the *z*-axis, w_{avg}, was normalized by the bulk average bundle velocity, W_o. The RMS velocity fluctuations, *w'*, were normalized by the local time-averaged *z*-component of velocity. Three axial locations in the bundle are shown at $3.7 \cdot D_H$ upstream of a spacer (blue), $3.5 \cdot D_H$ downstream of a spacer (red), and $23.6 \cdot D_H$ downstream of a spacer (green). All measurements have been corrected for measuring across velocity gradients as derived in Albrecht et al. (2003). Uncertainty limits are shown for the 95% confidence level on the pre-spacer measurements and are typical for the other axial locations. The estimated error limits are due primarily to uncertainty in the mass flow controllers used to meter the air into the assembly.

Velocities are not reported for positions between *x* of ~100 to 108.75 mm due to poor signal quality. The velocity profiles for the pre-spacer and mid-bundle are identical within experimental uncertainty and demonstrate a regular periodicity that correlates with the pin pitch as expected. The peak values of the post-spacer velocity profile are somewhat suppressed, indicating that part of the flow has diverted into the area between the spacer and the cell, or the wall subchannel. The normalized RMS fluctuations, commonly referred to as turbulence intensities, show repetitive non-zero values. A fully laminar treatment of this flow would require velocity fluctuations of zero. However, the split type mixing vanes imparted a significant wake into the flow. This wake is long lived, extending even to the mid-bundle measurement ($23.6 \cdot D_H$).

Fig. 7 shows the normalized mean velocity and RMS fluctuation profiles of the 217.5 mm cell for *Re* = 900. Again, axial locations in the bundle are shown for pre-spacer (blue), post-spacer (red), and mid-bundle (green). The uncertainty limits are again shown for the pre-spacer measurements. The uncertainties appear smaller in this graph because the magnitudes of the time-averaged and bulk velocities are approximately nine times greater while the absolute value of the uncertainty is unchanged.

The pre-spacer and mid-bundle time-averaged velocity profiles still demonstrate a semblance of periodicity with the pin pitch. The post-spacer is also periodic. However, the peaks and valleys now exhibit the strong influence of the repeating pattern of the split-type mixing vanes. The difference in

the maximum and minimum normalized velocities is reduced compared to *Re* = 100, indicating increased mixing. The normalized velocity fluctuations confirm the potential for enhanced flow mixing. The RMS values have greater magnitude than seen at *Re* = 100. Although somewhat harder to discern than in the mean velocity, the velocity fluctuations also appear to show the periodic influence of the spacer mixing vanes.

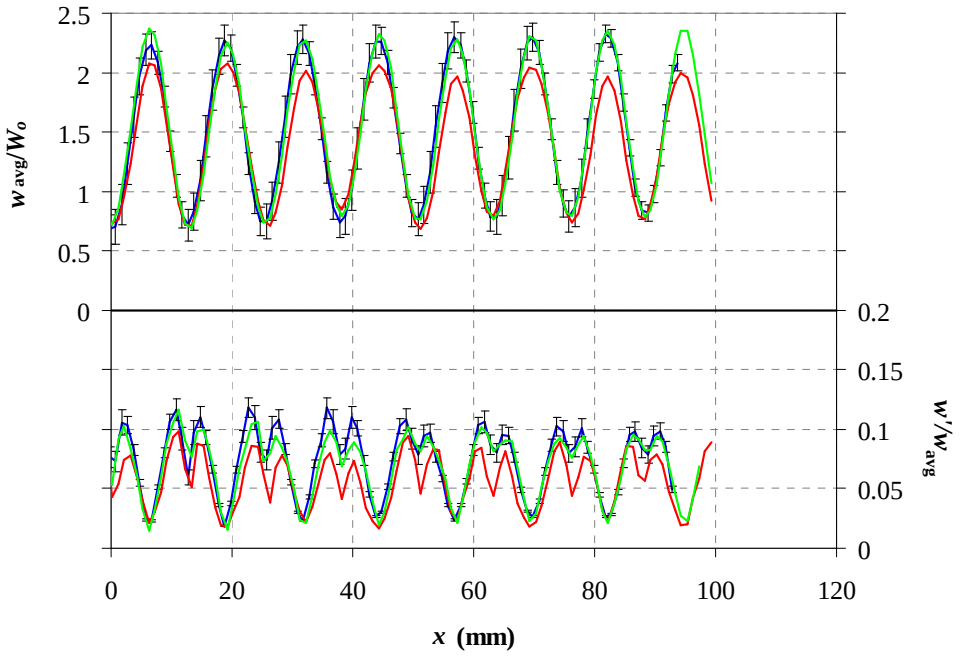

Fig. 6: Normalized mean velocity and RMS fluctuation profiles of the 217.5 mm cell for *Re* = 100 at pre-spacer (blue), post-spacer (red), and mid-bundle (green) axial locations.

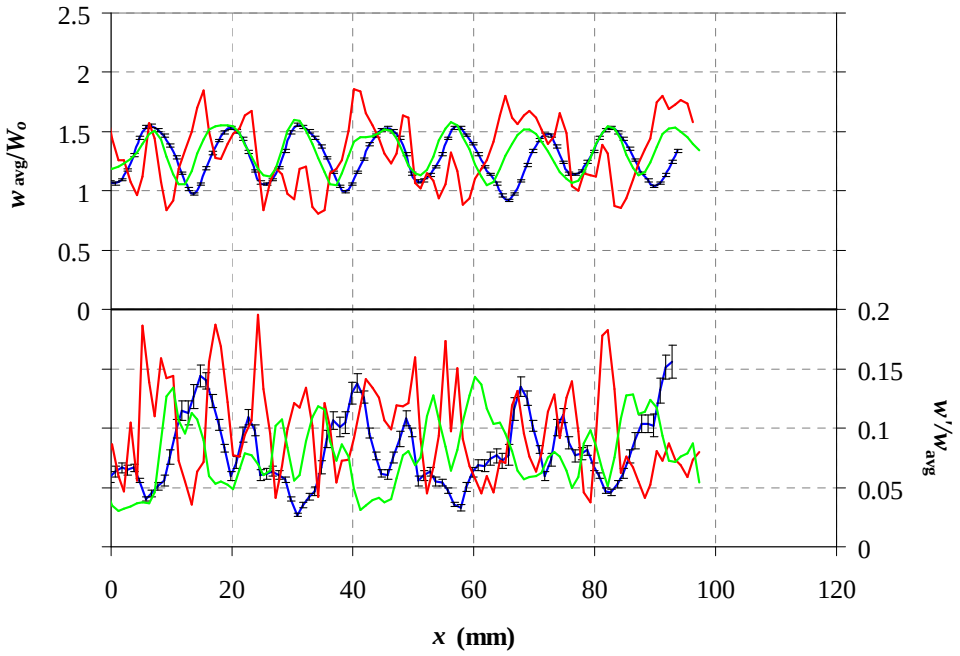

Fig. 7: Normalized mean velocity and RMS fluctuation profiles of the 217.5 mm cell for *Re* = 900 at pre-spacer (blue), post-spacer (red), and mid-bundle (green) axial locations.

The LDV profiles for the 226.6 mm cell and *Re* = 100 are shown in Fig. 8. The time-averaged velocity and RMS were normalized as before. The pre-spacer measurements (blue) are at an axial location of $3.2 \cdot D_H$ upstream of the spacer. The post-spacer measurements (red) are at $3.0 \cdot D_H$ downstream of the spacer, and the mid-bundle measurements (green) are at $20.5 \cdot D_H$ downstream of the spacer. The velocity of the flow in the wall subchannel is much higher for the 226.6 mm cell than the 217.5 mm, as expected. The profiles also suggest that a significant amount of cross flow has occurred downstream of the spacer, forcing flow into the wall subchannel from the bundle. This cross flow is also evident in the pre-spacer measurement as well, where the peak wall subchannel is elevated as compared to the mid-bundle. The increased RMS fluctuations at $x < 20$ mm for the pre-spacer and mid-bundle measurements were likely due to an increase in the photo-multiplier voltage and are not considered significant. The RMS fluctuations are periodic with the pin pitch and are comparable in magnitude to the *Re* = 100 case. As in the *Re* = 100 measurements, the fluctuations appear to be long-lived extending well into the mid-bundle and pre-spacer locations.

Fig. 9 gives the normalized velocity and RMS profiles for the 226.6 mm cell and *Re* = 900. The time-averaged velocity profiles for the mid-bundle and pre-spacer are periodic with the pin pitch with the maxima occurring in the middle of the subchannels and the minima at the points where the rods are closest to each other. The post-spacer measurements are also periodic. However, the cross flow created by the mixing vanes has redistributed flow away from the center of the subchannels.

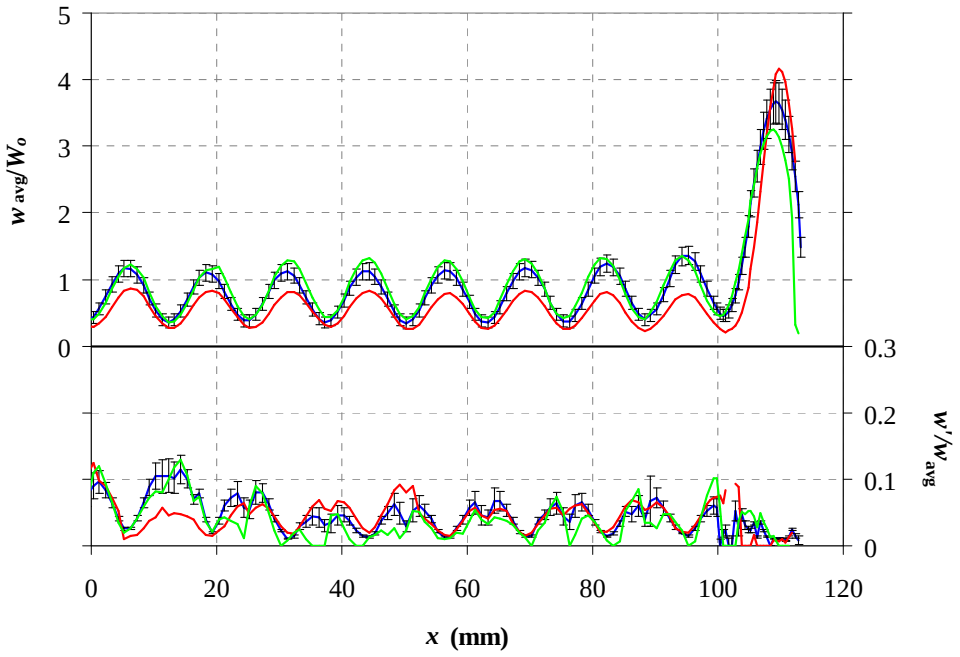

Fig. 8: Normalized mean velocity and RMS fluctuation profiles of the 226.6 mm cell for *Re* = 100 at pre-spacer (blue), post-spacer (red), and mid-bundle (green) axial locations.

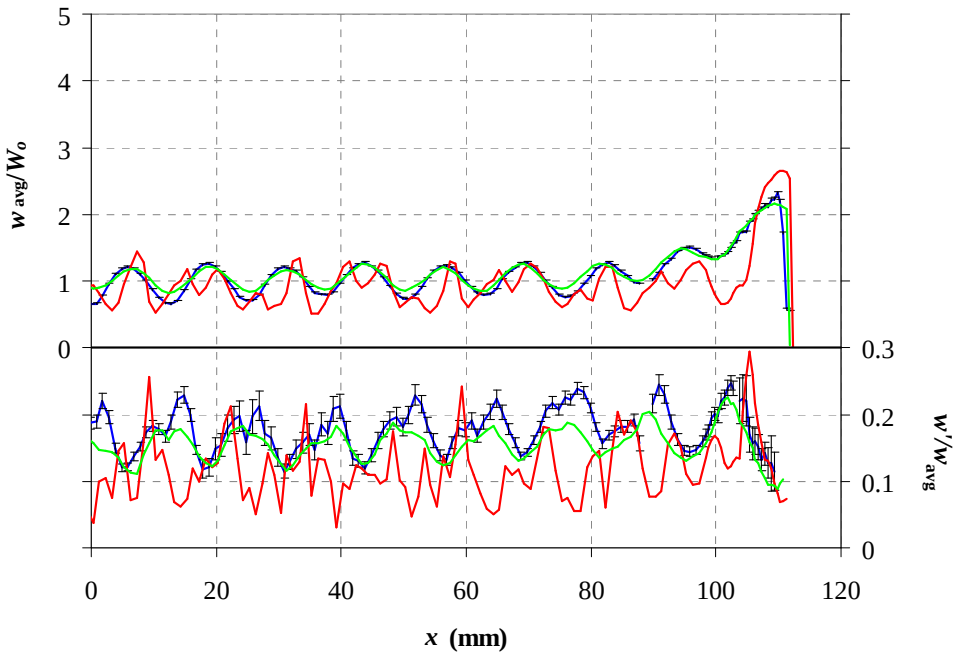

Fig. 9: Normalized mean velocity and RMS fluctuation profiles of the 226.6 mm cell for *Re* = 900 at pre-spacer (blue), post-spacer (red), and mid-bundle (green) axial locations.

4. CONCLUSIONS

Mean and fluctuations of the axial velocity component were measured in a commercial PWR fuel assembly in the traditionally defined laminar regime with laser Doppler velocimetry. Reynolds numbers of *Re* = 100 and 900 based on the bulk average assembly velocity and the hydraulic diameter were examined. Two storage cells of inner diameter 217.5 mm and 226.6 were used to represent commercially available dry storage casks and pool cell dimensions. Profiles were measured at three axial locations representing pre-spacer, post-spacer, and mid-bundle locations within the assembly.

The mean velocity profiles agreed reasonably with the fully-developed laminar solution values at *Re* = 100 for both cell sizes. The measured mean velocities at *Re* = 900 deviated from the idealized laminar case, demonstrating evidence of cross flow from the center of the subchannels. The increased cross flow leads to a more uniform velocity distribution as compared to the laminar profile. The velocity is underpredicted for both Reynolds numbers in the wall subchannel for the 226.6 mm cell. These effects demonstrate the influence of the spacers on the distribution of flow away from the idealized laminar case.

With the exception of the *Re* = 900 and 217.5 mm cell size, the velocity profiles for the pre-spacer and mid-bundle are identical within experimental uncertainty and demonstrate a regular periodicity that correlates with the pin pitch. The peak values of the post-spacer velocity profile at *Re* = 100 are somewhat suppressed, indicating that part of the flow has diverted into the wall subchannel. The post-spacer velocity profile at *Re* = 900 is also periodic. However, the peaks and valleys exhibit the strong influence of the repeating pattern of the split-type mixing vanes. The normalized RMS fluctuations show repetitive non-zero values. A fully laminar treatment of this flow would require velocity fluctuations of zero. However, the split type mixing vanes impart a significant wake into the flow. This wake is long lived, extending even to the mid-bundle measurement.

The flow within a bundle at Reynolds numbers conventionally considered laminar has been shown to deviate from the idealized laminar solution due to the complicating influence of the assembly spacers and intermediate fluid mixers. These spacers introduce wake and cross flow into the bulk flow that does not dissipate significantly within the bundle before encountering another spacer. Consideration

of these secondary flow effects must be incorporated into modelling efforts at low Reynolds numbers in order to capture the observed deviation from the laminar solution.

ACKNOWLEDGEMENTS

This work was conducted under Nuclear Regulatory Commission contract JCN# N6456. The authors would also like to thank Greg Koenig, Shane Adee, and Brandon Servantes for their efforts in constructing the test apparatus and conducting this test program.

REFERENCES

Albrecht, H.-E., Borys, M., Damaschke, N. and Tropea, C., 2003, *Laser Doppler and Phase Doppler Measurement Techniques*, Springer-Verlag, Berlin, Germany.

Caraghiaur, D., Anglart, H., and Frid, W., 2009, "Experimental Investigation of Turbulent Flow through Spacer Grids in Fuel Rod Bundles," *Nuclear Engineering and Design*, 239, 2013-2021.

Chang, S.K., Moon, S.K., Baek, W.P., and Choi, Y.D., 2008, "Phenomenological Investigations on the Turbulent Flow Structures in a Rod Bundle Array with Mixing Devices," *Nuclear Engineering and Design*, 238, 600-609.

Dominguez-Ontiveros, E.E. and Hassan, Y.A., 2009, "Non-Intrusive Experimental Investigation of Flow Behavior inside a 5×5 Rod Bundle with Spacer Grids using PIV and MIR," *Nuclear Engineering and Design*, 239, 888-898.

Durbin, S.G. and Lindgren, E.R., 2008, "Laminar Hydraulic Analysis of a Commercial Pressurized Water Reactor Fuel Assembly," SAND2008-3938, Sandia National Laboratories, Albuquerque, USA.

Lee, C.M. and Choi, Y.D., 2007, "Comparison of Thermo-Hydraulic Performances of Large Scale Vortex Flow (LSVF) and Small Scale Vortex Flow (SSVF) Mixing Vanes in 17×17 Nuclear Rod Bundle," *Nuclear Engineering and Design*, 237, 2322-2331.

Lindgren, E.R. and Durbin, S.G., 2010, "Measurement of Pressure Drops in Prototypic BWR and PWR Fuel Assemblies in the Laminar Regime," This Issue.

Rehme, K. and Trippe, G., 1980, "Pressure Drop and Velocity Distribution in Rod Bundles with Spacer Grids," *Nuclear Engineering Design*, 62, 349-359.